

Various Stacking Patterns of Two-Dimensional Molecular Assemblies in Hydrogen-Bonded Cocrystals: Insight into Competitive Intermolecular Interactions and Control of Stacking Patterns

Masaki Donoshita,^{*[a]} Yukihiro Yoshida,^{*[a]} Mikihiro Hayashi,^{[a],[b]} Ryuichi Ikeda,^[a] Susumu Tanaka,^[c] Yasuhisa Yamamura,^[d] Kazuya Saito,^[d] Shogo Kawaguchi,^[e] Kunihisa Sugimoto,^[e] and Hiroshi Kitagawa^{*[a]}

- [a] M. Donoshita, Dr. Y. Yoshida, Dr. M. Hayashi, Prof. R. Ikeda, Prof. H. Kitagawa
Division of Chemistry, Graduate School of Science
Kyoto University
Kitashirakawa-Oiwakecho, Sakyo-ku, Kyoto 606-8502 (Japan)
E-mail: donoshita@ssc.kuchem.kyoto-u.ac.jp, yyoshida@ssc.kuchem.kyoto-u.ac.jp, kitagawa@kuchem.kyoto-u.ac.jp
- [b] Dr. M. Hayashi
Faculty of Education
Nagasaki University
1-14 Bunkyo-machi, Nagasaki 852-8521 (Japan)
- [c] Prof. S. Tanaka
Department of Integrated Engineering
National Institute of Technology, Yonago College
4448 Hikona-cho, Yonago, Tottori 683-8502 (Japan)
- [d] Dr. Y. Yamamura, Prof. K. Saito
Department of Chemistry, Faculty of Pure and Applied Sciences
University of Tsukuba
Tsukuba, Ibaraki 305-8571 (Japan)
- [e] Dr. S. Kawaguchi, Dr. K. Sugimoto
Japan Synchrotron Radiation Research Institute (JASRI), SPring-8
1-1-1 Kouto, Sayo-cho, Sayo-gun, Hyogo 679-5148 (Japan)

Supporting information for this article is given via a link at the end of the document.

Abstract: We first demonstrate the rational control over the stacking patterns in two-dimensional (2D) molecular assemblies using chemical modification. A target system is a hydrogen-bonded cocrystal composed of 2-pyrrolidone (Py) and chloranilic acid (CA) with 2:1 composition (**PyCA**). X-ray crystallography revealed that various weak intersheet interactions give rise to a variety of metastable overlapping patterns comprised of the 2D assemblies mainly formed via hydrogen bonds, affording reversible and irreversible structural phase transitions. We successfully prepared cocrystals of Py and anilic acids bearing different halogens, in which 2D assemblies isostructural with those observed in **PyCA** exhibit various overlapping patterns. The order of stability for each overlapping pattern estimated using theoretical calculations of the intermolecular interactions did not completely coincide with those indicated by our experimental results, which can be explained by considering the entropic effect, i.e., the molecular motion of Py as detected using nuclear quadrupole resonance spectroscopy.

Introduction

Bulk materials have three-dimensional (3D) structures. However, upon microscopic observation, they consist of building blocks with lower dimensions, including two-dimensional (2D) sheets such as those observed in graphite, one-dimensional (1D) wires or tapes such as organic polymers, and zero-dimensional (0D) points like those found in molecular solids.^[1] Not only the components but also their assembling patterns are mainly responsible for the bulk properties because they modulate the

interactions between adjacent components. Therefore, it is highly desirable to establish a design methodology to control the assembling patterns of these building blocks. However, achieving such control is still challenging because the assembling patterns largely depend on multiple types of competitive interactions between the components, such as electrostatic, dipole-dipole, and dispersion interactions.^[2] A rational strategy is to focus on controlling the assembling patterns of higher-dimensional components because of their limited assembling manners.^[3] Notably, 2D materials have a dimensionality of one less than bulk 3D materials, resulting in the lowest degree of freedom in their assembling patterns when compared to other building blocks.

There are various 2D materials including inorganic, inorganic-organic hybrids, and organic ones, such as hexagonal boron nitride,^[4] transition metal dichalcogenides (MX₂),^[5] metal-organic frameworks (MOFs),^[6] graphene,^[7] and covalent organic frameworks (COFs).^[8] It is noteworthy that their stacking patterns have a significant effect on diverse properties of these materials, such as electronic conductivity,^[9] proton conductivity,^[10] and isomer selectivity.^[11] In addition, the mechanical properties associated with the change in the stacking patterns, such as thermo- and mechanosensitive^[12] and high deformability^[13] have been extensively studied over the last few decades.

Among them, 2D assemblies of organic molecules are an ideal platform for controlling stacking patterns because of their excellent designability in terms of their intermolecular interactions, such as π - π ,^[14] lone pair... π ,^[15] and CH... π .^[16] In

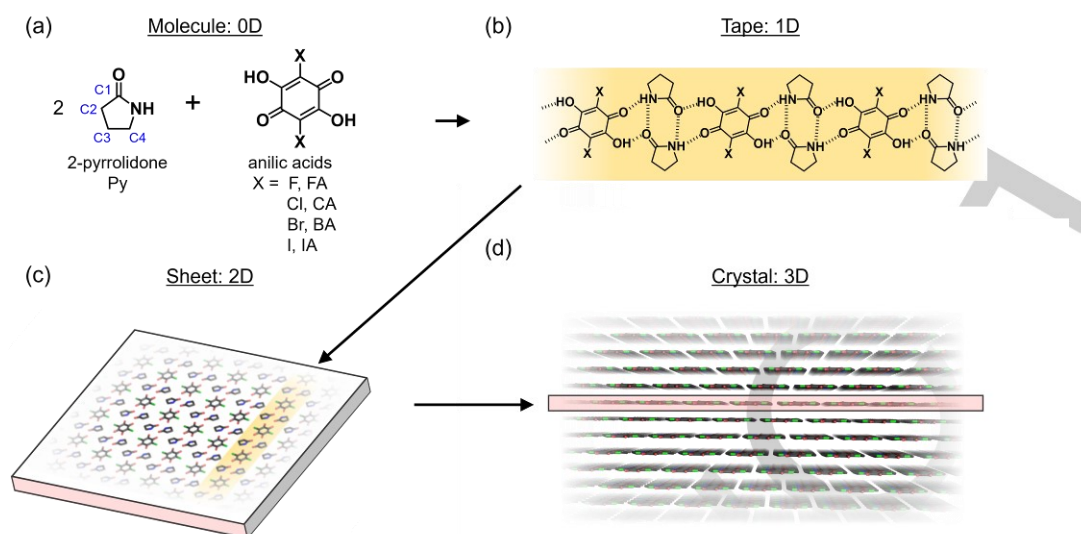


Figure 1. (a) Molecular structures (zero-dimension: 0D) of 2-pyrrolidone and anilic acids, which construct (b) one-dimensional (1D) hydrogen-bonded tape. (c) Two-dimensional (2D) sheet consisting of the hydrogen-bonded tapes and (d) the whole crystal structure of **PyCA** (High-B) formed by the stacking 2D sheets. Color code in (c) and (d): C, black; N, blue; O, red; Cl, green. Some parts of hydrogen atoms are omitted for clarity.

particular, hydrogen bonds are well-known strong intermolecular interactions with high directionality^[17] and various hydrogen-bonded self-assemblies with diverse dimensionalities have been constructed through careful molecular design.^[3,18] Such hydrogen-bonded assemblies are tolerant to chemical modification at molecular sites that are irrelevant for hydrogen bonding interactions. Therefore, by chemical modifications, one can possibly modulate the intermolecular interactions and hence the assembling patterns, while retaining the structure of the building blocks. However, there have been no reports describing the rational control of the assembling patterns of 2D organic assemblies using chemical modification.

A cocrystal composed of 2-pyrrolidone (Py) and chloranilic acid (CA) with a 2:1 composition [(Py)₂(CA), abbreviated **PyCA** hereafter] involves the hierarchically constructed self-assembly of 2D molecular sheets (Figure 1).^[19] In the 2D sheet, 1D tapes (Figure 1b) consisting of alternate Py dimers and CA connected via multiple hydrogen bonds are arranged in parallel with the van der Waals (vdW) interactions (Figure 1c). These 2D sheets are stacked via weak intermolecular π - π and Cl \cdots π interactions to form 3D crystals (Figure 1d). We have previously reported the successive structural phase transitions accompanied by a drastic translation of the sheets (ca. 7 Å) upon varying the temperature.^[19b] Because this indicates the robust nature of the 2D assemblies and comparable intersheet interaction energies of the overlapping patterns, this system is suitable for the present study. In addition, single-crystal X-ray diffraction (SCXRD) measurements suggested that conformational disorder of Py molecules is related to a phase transition. Such structural flexibility is apparently unique to molecular crystals and has become increasingly important in materials science. Various physical properties correlated to the flexibility, such as ferroelectricity,^[20] spin-crossover,^[21] and superconductivity,^[22] have been reported. However, there are no reports that discuss the entropic effect associated with molecular flexibility on the changes observed in the assembling patterns of 2D assemblies.

In this paper, on the basis of experimental and computational approaches, we first demonstrate the control of the overlapping patterns of robust molecular 2D assemblies

using halogen substitution of a component molecule and identify the factors that govern the pattern from the viewpoints of their intermolecular interactions and molecular flexibility. Prior to the discussion on halogen substitution, we show the structural phase transition behavior of **PyCA** including a new polymorph recently obtained during careful monitoring of the transition of the crystals, which prompted us to investigate the structural effects of halogen substitution.

Results and Discussion

1. Structural phase transition behavior of **PyCA**

1.1 New polymorph and energy diagram. We have previously reported the existence of three polymorphs (High-A, Low-B, and High-B) in **PyCA**.^[19b] Here, the suffixes, A or B, for each polymorph represent the different modes of their stacking patterns; High-A involves two types of overlapping patterns of the sheets that are arranged alternately, whereas Low-B and High-B involve one overlapping pattern that is arranged uniformly (Figure 2b–d, top). It should be noted that the three polymorphs are related by a successive transition of High-A (298 K) \rightarrow Low-B (100 K) \rightarrow High-B (298 K) upon changing the temperature.

Variable-temperature single-crystal X-ray diffraction (VT-SCXRD) experiments on several crystals of the High-A polymorph of **PyCA** upon cooling from 298 K to 100 K revealed the existence of a new polymorph at 100 K. This polymorph also possesses a 2D layered structure and the molecular arrangement within the 2D sheet was the same as that of the three previously reported polymorphs. The new polymorph was revealed to have an alternating stacking mode similar to High-A (Figure 2a,b, top), and we therefore refer to the new polymorph as Low-A hereafter. Low-A shows a reversible transition to High-A at around ca. 120 K, in contrast to the irreversible High-A \rightarrow Low-B transition. This transition between High-A and Low-A can be regarded as a first-order transition because of the thermal hysteresis observed in VT-SCXRD (Figure S1). The crystallographic data of Low-A are listed in Table S1 and the

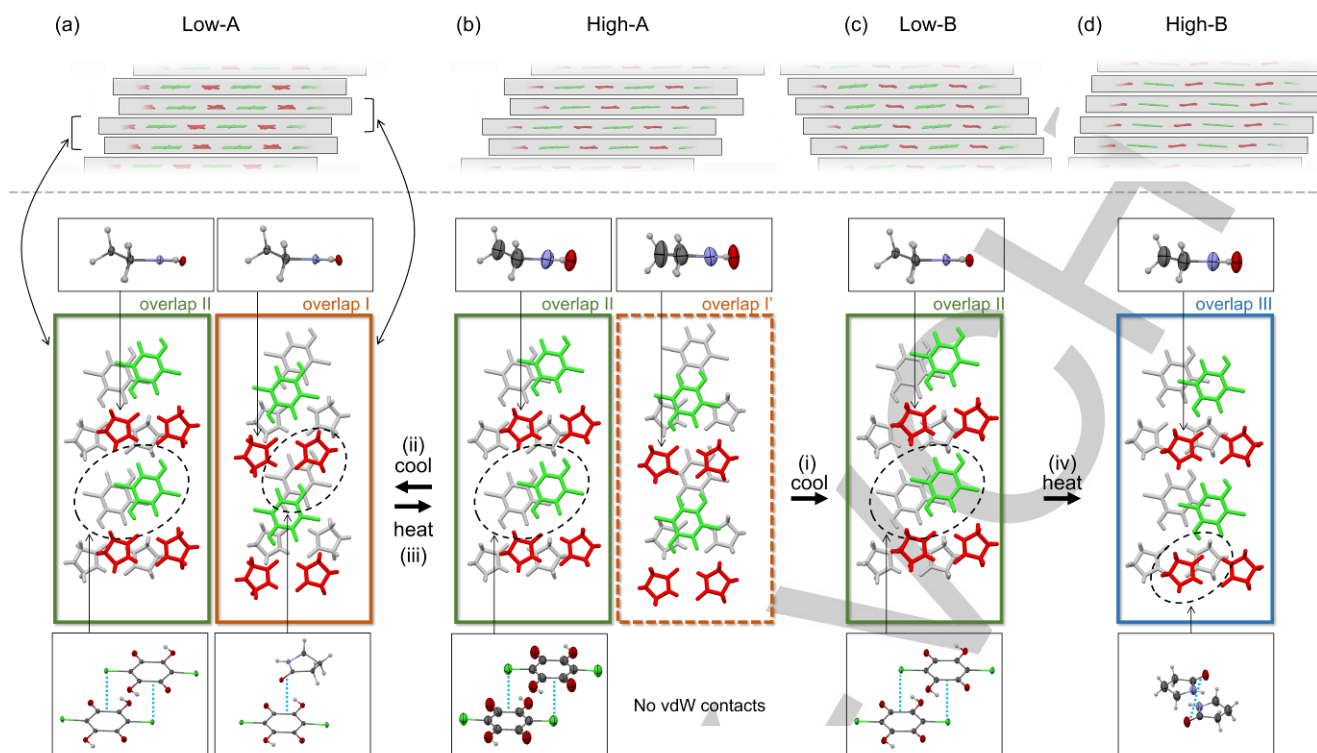


Figure 2. Side-view of stacked tapes (top panel) and face-view of two stacked tapes (bottom panel) of **PyCA** for (a) Low-A consisting of alternating overlap I and II at 100 K, (b) High-A consisting of alternating overlap I' and II at 298 K, (c) Low-B consisting of overlap II at 100 K, and (d) High-B consisting of overlap III at 298 K. In the top panels, Py and CA molecules appear in red and green, respectively. In the bottom panels, the Py and CA molecules indicated in red and green, respectively, are placed in front of the gray molecules. The insets in bottom panels show the conformation of Py (upper) and positional relationship of each molecular pair having intersheet vdW contacts (lower). Molecules in the insets are drawn with thermal ellipsoids with 50% probability (gray, C; white, H; purple, N; red, O; green, Cl).

overlapping patterns of the 2D assemblies in Low-A are shown in Figure 2 with those of other polymorphs for comparison.

In **PyCA**, four types of overlapping patterns (overlap I, I', II, and III) between two adjacent sheets exist. In overlap I' (Figure 2b, bottom right), the adjacent sheets overlap with a shift of ca. 4.7 Å and there are no intersheet vdW contacts (see Figure S3 for detailed figures of the overlapping patterns).^[23] Overlap I (Figure 2a, bottom right) involves a similar overlapping pattern to overlap I' where the adjacent sheets overlap with a shift of ca. 3.6 Å, but an intersheet vdW contact exists between Py and CA. In overlap II (Figure 2a,b, bottom left and 2c), the adjacent sheets overlap with a shift of ca. 3.4 Å and an intersheet vdW contact between the CAs exists. Overlap III (Figure 2d) involves sheets overlapping each other with a shift of ca. 3.7 Å and has an intersheet vdW contact between Pys. In Low-B and High-B, all the adjacent sheets overlap in the manner of overlap II and III, respectively, whereas the sheets in High-A and Low-A are arranged in an alternating manner of overlap I' and II and overlap I and II, respectively (Figure 2, top).

In the High-A → Low-A transition, overlap I' is transformed into overlap I via the translation of the adjacent sheets along the direction parallel to the C=O bonds in CA by ca. 1.5 Å. This results in the formation of an intersheet vdW contact between Py and CA. In addition, the disappearance of the structural disorder of Py was observed during the High-A → Low-A transition, similar to the High-A → Low-B transition.^[19b] That is, one of the non-equivalent Py molecules shows a significant conformational disorder between the two envelope conformations bending up and down, and the equivalent isotropic atomic displacement parameter ($U_{\text{eq}} = 0.0830(11) \text{ \AA}^2$ at

298 K) of the 4-positioned carbon (C3 in Figure 1a) is significantly larger than the other carbon atoms in High-A (Figure 2b, inset), whereas that of the corresponding carbon in Low-A is small ($U_{\text{eq}} = 0.0155(5) \text{ \AA}^2$ at 100 K, Figure 2a, inset and Figure S2). It is noteworthy that this disorder in the Py skeleton was revealed to be dynamic using nuclear quadrupole resonance (NQR) spectroscopy, as will be discussed in Section 2.4. The High-A ↔ Low-A transition can be regarded as a transition associated with the balance between the entropic term of Gibbs energy (G) related to the structural disorder and the enthalpic

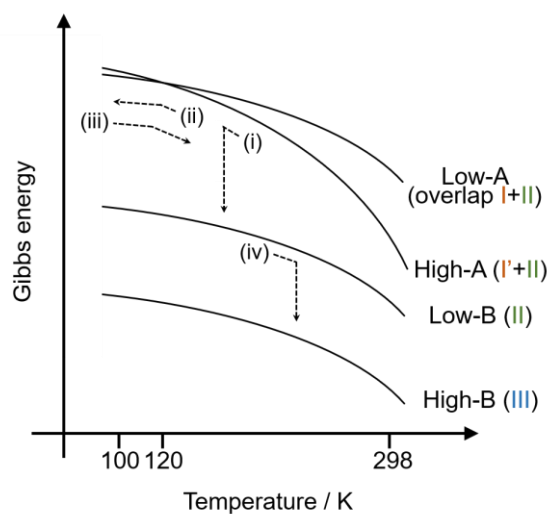


Figure 3. A schematic representation of the Gibbs energy diagram for the four polymorphs of **PyCA** as a function of temperature. The dashed arrows represent the observed transitions.

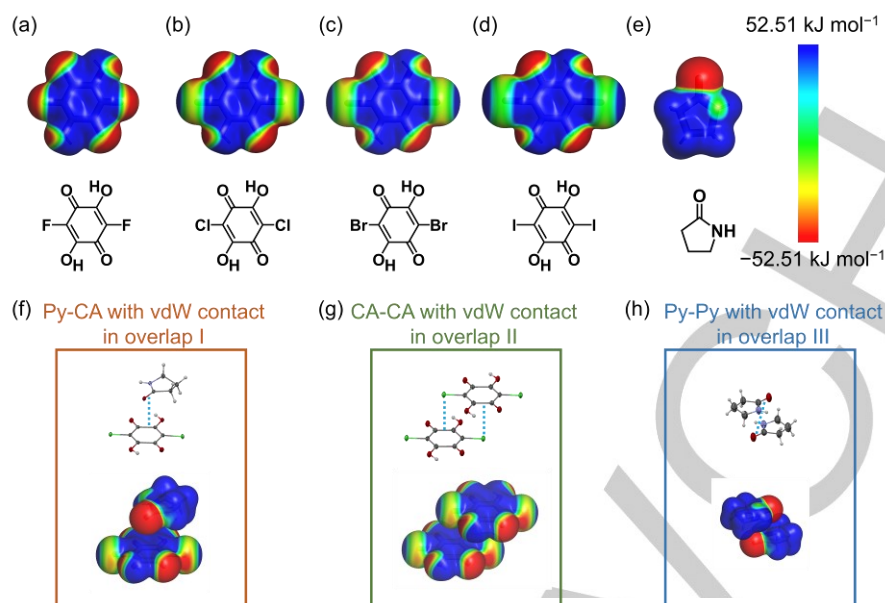


Figure 4. The calculated MP2/aug-cc-pVDZ(-PP) level surface electrostatic potentials obtained for (a) FA at 100 K, (b) CA in High-B at 100 K, (c) BA at 100 K, (d) IA at 100 K, and (e) Py in High-B at 100 K computed on the 0.005 electron bohr⁻³ contour of the electronic density (blue, positive region; green, transition region; red, negative region). Color range (kJ mol⁻¹): blue, > 52.51; red, < -52.51. The molecular structures (top) and surface electrostatic potentials (bottom) of the molecular pair with intersheet vdW contacts consisting of (f) Py and CA in Low-A at 100 K, (g) CA and CA in Low-B at 100 K, and (h) Py and Py in High-B at 100 K. The bottom figures are drawn by combining surface electrostatic potentials calculated for the individual monomers. Computational methods are the same as those for (a)–(e).

term related to the intersheet interactions.

To gain an understanding of the energetic relationship among the polymorphs, variable-temperature powder XRD (PXRD) experiments of High-A was performed (Figure S4). The coexistence of irreversible High-A → Low-B → High-B and reversible High-A ↔ Low-A transitions were observed upon cooling and subsequent heating (298 K → 100 K → 298 K). Notably, the transition temperature of the Low-B → High-B transition upon heating (190 K) was higher than that of the High-A → Low-B transition upon cooling (170 K), implying that the Gibbs energy–temperature curves for High-A and Low-B do not cross. Given that High-B does not show a phase transition upon cooling,^[19b] the energy diagram of the four polymorphs can be drawn, as shown in Figure 3.

The disorder of Py can be regarded as one of the possible origins of trapping of the metastable High-A, which affords the two series of the transitions. As the disorder of Py disappears upon cooling, High-A can transform into thermodynamically more stable Low-B with a significant change in the stacking patterns from overlap I' to II ((i) in Figure 2 and 3). However, this change needs to be accompanied by a large translation of the sheets (ca. 7 Å) and therefore, some of the High-A crystals may fail to transform into Low-B and instead transform to Low-A at the cross point of the energy curves of High-A and Low-A ((ii) in Figure 2 and 3). The factor determining which crystals have a Low-A or Low-B structure at low temperature is unclear at this stage, although the crystal quality may be an important factor because the lattice imperfection such as defects might preferentially disturb the irreversible transition accompanied by the significant translation of 2D sheets.

Accordingly, we can conclude that High-A, Low-B, and Low-A are all metastable states and that the only stable phase is High-B.

1.2 Nature of the intersheet intermolecular interactions. To investigate the nature of the intersheet interactions, we calculated the surface electrostatic potential of each component

molecule at the MP2/aug-cc-pVDZ level of theory (Figure 4, top). In CA (Figure 4b), the central benzene ring is positively charged. On the other hand, the O and Cl atoms in the peripheral parts are negatively charged, whereas the H atoms are positively charged, as expected from the atomic electronegativities. For Py (Figure 4e), the O and N atoms are negatively charged, whereas the C and H atoms are positively charged. As mentioned above, SCXRD measurements revealed that intersheet vdW contacts are present between Py and CA in overlap I, CA and CA in overlap II, and Py and Py in overlap III, in which the oppositely charged molecular sites approach each other owing to the electrostatic interactions (Figure 4f–h). Notably, the CA⋯CA contact in overlap II originates from the lone pair⋯π interaction, where the negatively charged halogen and the positively charged benzene ring (i.e., π-hole) are attracted to each other. Such interactions based on π-holes have been recently recognized and extensively studied in the field of crystal engineering.^[24]

In addition to the above-mentioned intersheet interactions with vdW contacts, it is most likely that the pairs with no short interatomic contacts are also responsible for determining the relative stabilities of each overlapping pattern.^[25] Thus, we have considered entire intersheet interaction energies for an isolated pair of sheets by taking the sum of the intermolecular interaction energies for intersheet pairs of molecules. We employed all molecular pairs with a center-to-center distance up to $d = 16$ Å based on the d dependence of intermolecular interaction energies (see Figure S5–7). The calculations were performed at the SAPTO/jun-cc-pVDZ level of theory, and the results are given as a quantity per mole of **PyCA** (i.e., total one mole in two sheets) in the following.

The interaction energies for overlap I, II, and III were calculated to be -55.83 kJ mol⁻¹ (Low-A at 100 K), -56.54 kJ mol⁻¹ (Low-B at 100 K), and -59.34 kJ mol⁻¹ (High-B at 100 K) (Figure 5), respectively (intersheet distance: 3.27, 3.42, and 3.34 Å, respectively). It is noteworthy that the division of the whole

energy in each pair, that is, Py-Py, Py-CA, and CA-CA, showed a marked difference in the nature of the stacking forces (Figure 5). In overlap I, the Py-CA term is the major component (81.0%) of the intersheet interactions, whereas in overlap III, the Py-Py term is the majority (54.2%). In overlap II, the contributions from Py-Py and CA-CA are comparable to each other (45.4 and 34.4%, total 79.9%), which constitute the majority of the intersheet interactions.

The difference in the energetic contribution among overlap I, II, and III prompted us to study the chemical modification of one component molecule to control the stacking patterns. Given that the heavier halogen has larger atomic polarizability (F, 0.557; Cl, 2.16; Br, 3.11; I, 5.35 Å³),^[26] it is intuitively expected that replacing the chlorine in CA with a heavier halogen will lead to an increase in the interaction energies of the CA-related terms, that is, Py-CA and CA-CA, and thus overlap I or II exhibiting a larger contribution from the CA-related terms become more stable than overlap III. In the following section, therefore, we present the effect of halogen substitution on the stacking pattern using both experimental and computational approaches.

2. Effect of halogen substitution.

2.1 Synthesis and crystal structures of halogen-substituted cocrystals.

The combination of anilic acids bearing different halogens [XA (FA; X = F, BA; X = Br, and IA; X = I in Figure 1a)] with Py gave their corresponding cocrystals (**PyXA**), that is, **PyFA**, **PyBA**, and **PyIA** with the same composition as **PyCA**. Cocrystallization was performed using an acetonitrile solution containing Py and XA. For each cocrystal, two methods, that is, cooling of the hot solution and evaporation of the solution at room temperature, were conducted and both afforded the same crystal structure (see Experimental and computational methods in Supporting information for details). This is in contrast to the case observed for **PyCA**, where the cooling and evaporation processes provided metastable High-A and stable High-B phases, respectively. Despite the different vdW radii of the halogens (Figure 6a), all the cocrystals involve the 2D assemblies same as **PyCA** (Figure 6b–e). In addition, the halogen-substituted cocrystals showed no phase transitions in

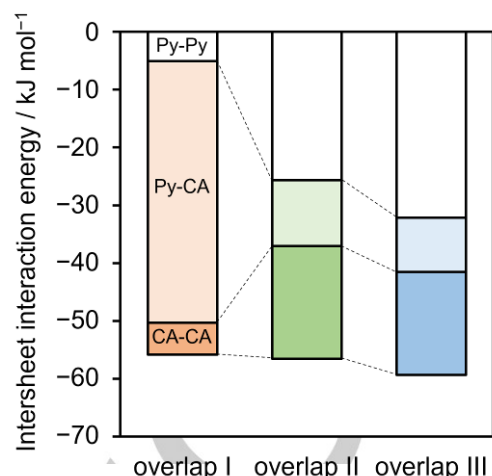


Figure 5. Intersheet interaction energies of overlap I (left), II (center), and III (right) in **PyCA** at 100 K. For each overlapping pattern, the contribution from the molecular pairs of CA-CA, Py-CA, and Py-Py are shown by dark, light, and no shading areas, respectively. The intersheet interaction energies were calculated for an isolated pair of sheets. The results are given as quantities per mole of **PyCA**.

the temperature range studied (100–373 K)^[27], in contrast to the case of **PyCA**. The crystallographic data of the cocrystals are listed in Table S1 and S2.

However, the overlapping patterns were indeed different for each cocrystal, as expected. The face-views of two hydrogen-bonded tapes in two adjacent layers are displayed in Figure 7, together with those of **PyCA**. **PyBA** and **PyIA** adopt a uniform stack of overlap II, which is isomorphous to Low-B of **PyCA**. Here, the formation of overlap II in **PyBA** and **PyIA** is consistent with the expectation based on our calculations (see Section 1.2). On the other hand, **PyFA** adopts a uniform stack of overlap I, which is the same as one of the overlapping patterns of Low-A observed for **PyCA**.

Notably, **PyFA** and **PyCA** showed a fair cleavage property parallel to the 2D sheets, which even affords rather thin plates (Figure S8). We note that the fabrication of organic thin plates is

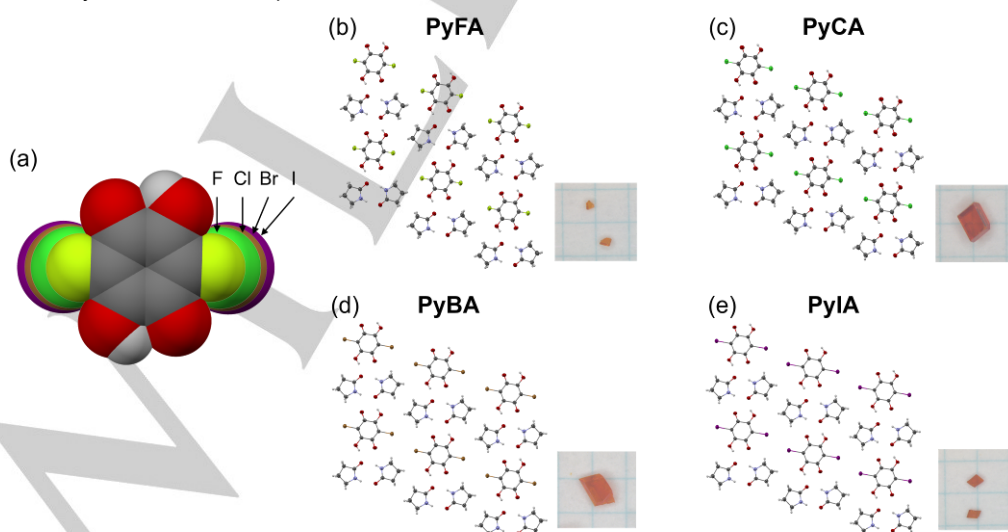


Figure 6. (a) Molecular models of the XAs based on the structure of CA in High-B of **PyCA** (298 K), in which the size of the spheres corresponds to the van der Waals radius of each atom.^[23] For FA, BA, and IA, Cl atoms of CA were replaced with F, Br, and I, respectively. The C–X bond lengths were modified using the literature values (F. H. Allen, D. G. Watson, A. Brammer, A. G. Orpen, R. Taylor, *Typical interatomic distances: organic compounds*, in *International Tables for Crystallography Volume C: Mathematical, physical and chemical tables*, 2nd Ed. (Ed.: E. Prince), Kluwer Academic Publishers, Dordrecht, 1999, pp. 782–803.). Two-dimensional sheets of (b) **PyFA**, (c) **PyCA** (High-B), (d) **PyBA**, and (e) **PyIA** at 298 K. The molecules are drawn with thermal ellipsoids with 50% probability (gray, C; white, H; purple, N; red, O; yellow, F; green, Cl; orange, Br; magenta, I). The inset shows the photograph of each cocrystal on millimeter marked paper.

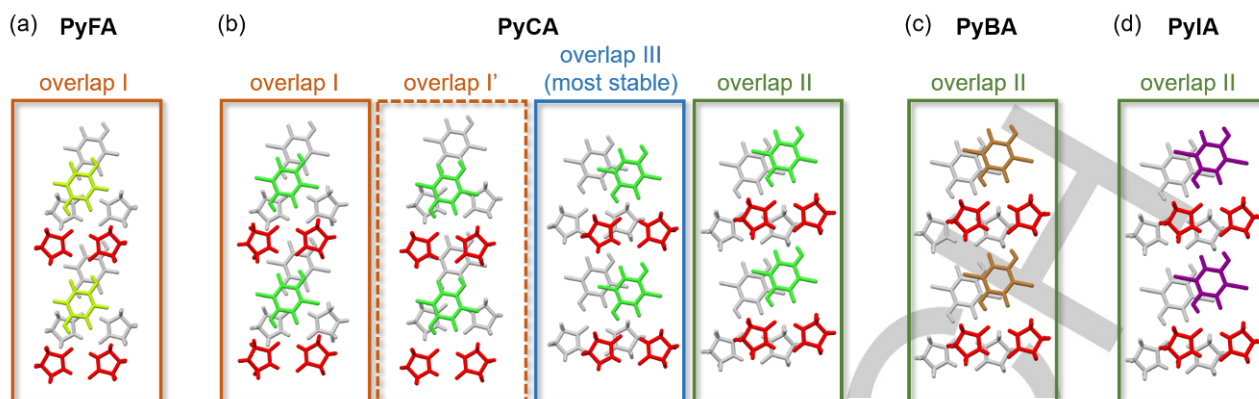


Figure 7. Face-view of two stacked tapes of (a) **PyFA**, (b) **PyCA**, (c) **PyBA**, and (d) **PyIA**. For **PyCA**, overlap I, I', II, and III were extracted from the crystal structures of Low-A at 100 K, High-A at 298 K, Low-B at 100 K, and High-B at 298 K, respectively. Colored molecules (red, Py; yellow, FA; green, CA; orange, BA; magenta, IA) are placed in front of the gray molecules.

an important topic in the field of organic photonics.^[28]

2.2 Discussion on the appearance of overlap II in PyBA and PyIA. Here, we discuss why the substitution of a halogen from Cl to heavier Br or I leads to the change in the stable overlapping pattern from overlap III to II. As mentioned in Section 1.2, a possible scenario for the change in the stability of stacking patterns is that the substitution with a heavier halogen induces an increase in the atomic polarizability, followed by an increase in the XA-related intermolecular interactions. In this case, overlap II with a larger contribution from the XA-related interactions can become more stable than overlap III (Figure 5).

To confirm the increase in the XA-related terms upon halogen substitution, we calculated the intersheet interactions of **PyBA** and **PyIA** based on the crystal structures at 100 K (intersheet distance: 3.47 and 3.53 Å, respectively). As shown in Figure 8a, the Py-Py term remains almost unchanged with respect to halogen substitution (-25.69 , -26.32 , and -26.27 kJ mol⁻¹ for **PyCA**, **PyBA**, and **PyIA**, respectively), whereas the XA-XA term is more significantly influenced by the halogen substitutions (-19.48 , -21.33 , and -24.71 kJ mol⁻¹ for **PyCA**, **PyBA**, and **PyIA**, respectively).

To elucidate the origin of the increase in the XA-related terms, we performed energy decomposition analysis of the XA-

XA terms for **PyCA**, **PyBA**, and **PyIA**, based on the symmetry-adapted perturbation theory (SAPT) method,^[29] which can partition the molecular interactions into electrostatic, induction, dispersion, and exchange terms (see Experimental and computational methods in Supporting information for details). As shown in Figure 8b, the dispersion term (-22.68 , -25.47 , and -32.38 kJ mol⁻¹ for **PyCA**, **PyBA**, and **PyIA**, respectively) was more strongly influenced by the halogen substitutions than the electrostatic term (-12.94 , -14.12 , and -16.62 kJ mol⁻¹). This indicates that the enhancement in the induced dipole, rather than a change in the intramolecular charge distribution in the unperturbed monomers, is the primary cause of the increased XA-related term upon halogen substitution. Notably, this result is consistent with the calculations of surface electrostatic potentials showing no significant change in the charge distribution due to halogen substitution (Figure 4a–d).

2.3 Discussion on the appearance of overlap I in PyFA. Contrary to the case of **PyBA** and **PyIA**, the substitution with lighter F is expected to result in a decrease in the polarizability and XA-related terms. Thus, overlap III must be the most stable overlapping pattern in **PyFA** because it has the largest intersheet interactions and the smallest ratio of XA-related terms in **PyCA** (Figure 5). However, overlap I was revealed to be most

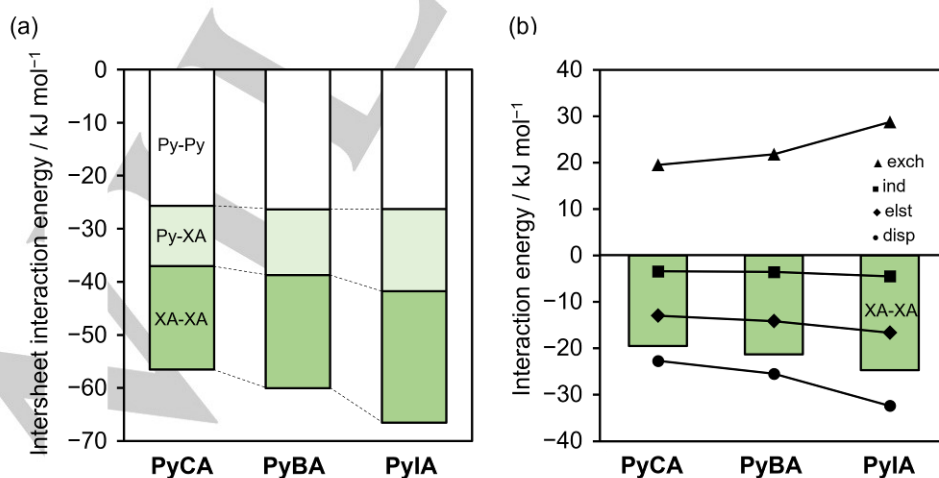


Figure 8. (a) Intersheet interaction energy of overlap II for **PyCA** (Low-B, left), **PyBA** (center), and **PyIA** (right) at 100 K. For each cocrystal, dark, light, and no shading show the contribution from the molecular pairs of Py-Py, Py-XA, and XA-XA, respectively, where XA = CA, BA, or IA. (b) Partitioned intersheet interaction energies obtained for the XA-XA molecular pairs in overlap II (exch, exchange; elst, electrostatic; ind, induction; disp, dispersion). The green bar graphs show the total interaction energies, namely the sum of all the components. The intersheet interaction energies were calculated for an isolated pair of sheets. The results are given as quantities per mole of **PyXA**.

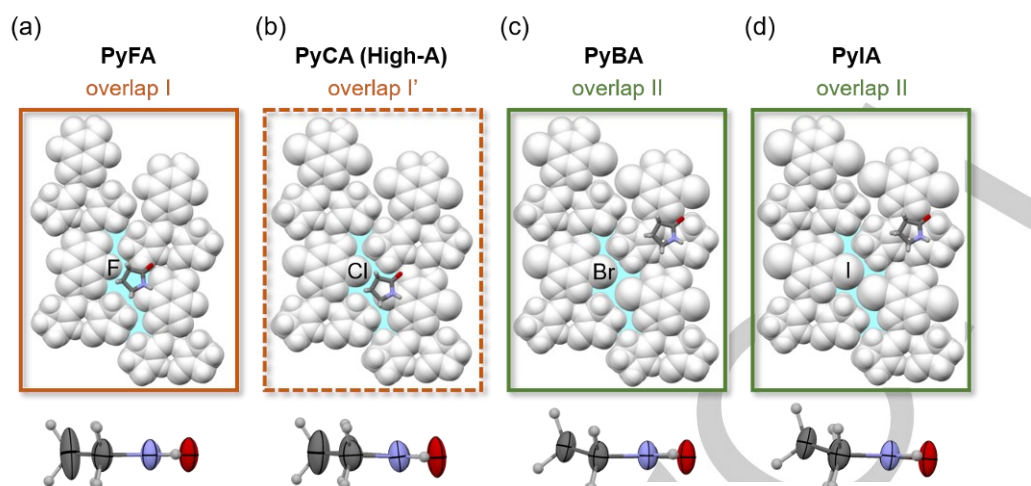


Figure 9. Intrashet molecular packing viewed perpendicular to the molecular plane (top) and side-view of Py (bottom) in (a) **PyFA**, (b) **PyCA** (High-A), (c) **PyBA**, and (d) **PyIA** at 298 K. In the top panel, a Py molecule drawn by a colored capped stick model (gray, C; white, H; purple, N; red, O) is placed in front of a sheet drawn using a white space filling model showing the vdW surface. The pale blue colored area shows the cavities formed between the two tapes. In the bottom panel, a Py molecule is drawn with thermal ellipsoids with 50% probability. Atoms are colored in the same way as Py in the top panel.

stable in **PyFA**. To clarify the reason, we focused on the conformational disorder of Py. Because the High-A \leftrightarrow Low-A transition in **PyCA** is a transition between Low-A, which adopts overlap I with intersheet vdW contacts and without disorder, and High-A, which adopts overlap I' without intersheet vdW contacts and with disorder, it is apparent that the entropic term associated with disorder compensates for the enthalpic term associated with intersheet interactions in **PyCA**. Given that such a disorder was also observed in **PyFA** with overlap I, as evidenced by the elongated thermal ellipsoid ($U_{eq} = 0.1013(14)$ Å² at 298 K) of the 4-positioned carbon in Py (Figure 9a bottom), the entropic contribution may stabilize overlap I with an expected smaller enthalpic contribution than that of overlap III in **PyFA**. To verify the above considerations, we roughly estimated the contribution from the entropic term. Assuming the disorder of Py between the two conformations (two envelope conformations bending up and down), one Py molecule in motion affords the entropy of $k \ln 2$, where k is the Boltzmann constant. Considering that half of Py molecules is dynamically active in High-A of **PyCA** [= (Py)₂(CA)], the entropy resulting from the motion is $N_A k \ln 2 = 5.76$ J K⁻¹ mol⁻¹ per mole of **PyCA**, where N_A is the Avogadro's number. Notably, the stabilization owing to this entropy reaches a few kJ mol⁻¹ in the temperature range studied (100–300 K) and the value is of the same order of magnitude as the energy difference between overlap I and III in **PyCA** (3.51 kJ mol⁻¹). In the case of **PyFA**, all of the Py molecules show the conformational disorder, and therefore, the entropic gain is twice the above estimation.

Notably, the pronounced conformational disorder of Py in **PyFA** and **PyCA** (High-A) arises from trapping at the cavity between the tapes in an adjacent sheet (Figure 9a,b, top). Because the cavity is shrunk upon substitution with heavier halogens with larger vdW radii (Figure 9c,d, top), the disorder of Py and resulting entropic gain should be negligible even if overlap I or I' were realized in **PyBA** and **PyIA**.

2.4 Evaluation of the motion of Py. In this study, we succeeded in controlling the stacking patterns of 2D layered molecular crystals, **PyXA**. The change in the XA-related intersheet interactions induced by changing the polarizability of XA is a key factor in controlling the stacking patterns. Moreover, structural disorder is also a primary factor determining the

stacking patterns. However, the current evidence for the disorder of Py is only the result of SCXRD, which does not usually discriminate between the static and dynamic disorder in most cases. Hence, we used the nuclear magnetic resonance technique, which is a powerful tool for investigating molecular dynamics because its resonance frequency is comparable to the low frequency range of molecular motion. We initially conducted ¹H NMR (nuclear magnetic resonance) experiments of polycrystalline **PyCA** sample and found that it has a very long spin-lattice relaxation time (T_1) of ca. 600 s (Figure S9). We then performed ³⁵Cl NQR experiments to reduce the measurement time. NQR spectroscopy, which is a measurement for probing the electric field gradient at the nucleus site, is sensitive to the local environment and might detect the dynamical motion of Py even through the Cl nuclei in the CA molecules.^[30]

We carried out variable-temperature ³⁵Cl NQR measurements (298 K \rightarrow 77 K \rightarrow 298 K) of polycrystalline **PyCA**. At room temperature, two signals ascribed to crystallographically non-equivalent Cl sites in High-A were observed (Figure 10a, inset). Given that distinct signals were observed in High-A, it is obvious that the disorder of Py observed using XRD is dynamic because static disorder would result in the disappearance of the NQR signals due to the disturbance of the electric field around resonant Cl.

Upon cooling, one signal for Low-B began to appear at around 165 K, while the signals for High-A faded (Figure S10). In the subsequent heating process, one signal for High-B emerged at around 190 K and became intense, while the signal for Low-B gradually disappeared. The signals attributable to Low-A were not detected, probably because the High-A \leftrightarrow Low-A transition occurs with very low probability.

The temperature dependence of T_1 for High-A and Low-B during the cooling process is shown in Figure 10 with the results obtained for High-B. The temperature dependence of Low-B and High-B is well fitted using the following equation considering the lattice vibration:^[31]

$$T_1^{-1} = aT^n$$

$$(a = 5.5 \pm 1.5 \times 10^{-5} \text{ s}^{-1} \text{ K}^{-n}, n = 2.30 \pm 0.06 \text{ for Low-B};$$

$$a = 3.6 \pm 0.9 \times 10^{-5} \text{ s}^{-1} \text{ K}^{-n}, n = 2.35 \pm 0.05 \text{ for High-B}).$$

On the other hand, the T_1 value for High-A showed a downward deviation from the above equation at around 270–150

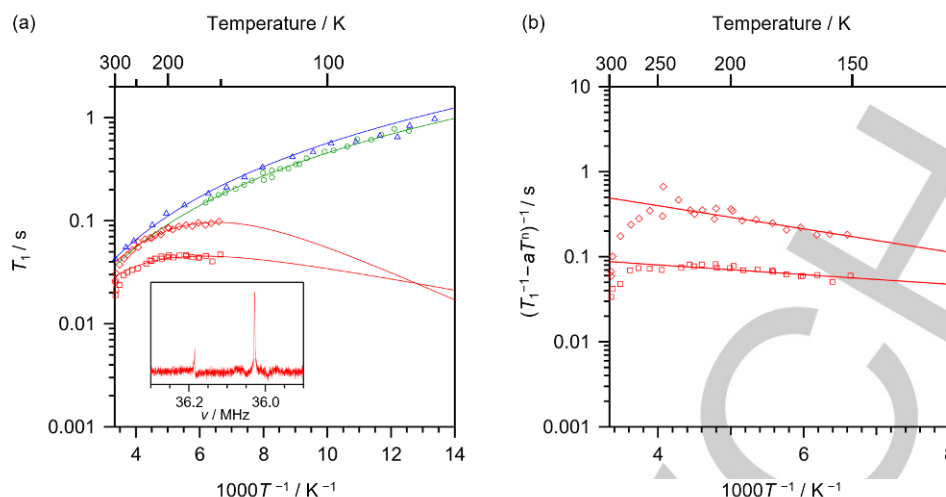


Figure 10. (a) Temperature dependence of T_1 in ^{35}Cl NQR for **PyCA**. Red squares (\square) and diamonds (\diamond) represent the data for High-A. Green circles (\circ) and blue triangles (Δ) represent the data for Low-B and High-B, respectively. For solid lines, see text. The inset shows the spectrum at room temperature (292 K). (b) Temperature dependence of $(T_1^{-1} - aT^n)^{-1}$ following Arrhenius-type behavior.

K. The temperature dependence is well explained using the following equation, assuming the coexistence of the lattice vibration and a molecular motion following an Arrhenius-type relaxation with an activation energy of ca. 2 kJ mol $^{-1}$.^[31,32]

$$T_1^{-1} = aT^n + b\exp(E_a/RT)$$

$$(a = 3.6 \times 10^{-5} \text{ s}^{-1} \text{ K}^{-n}, n = 2.35, b = 7.1 \pm 1.7 \times 10^{-1} \text{ s}^{-1},$$

$$E_a = 2.6 \pm 0.4 \text{ kJ mol}^{-1}$$

$$\text{and } a = 3.6 \times 10^{-5} \text{ s}^{-1} \text{ K}^{-n}, n = 2.35, b = 7.3 \pm 0.9 \text{ s}^{-1},$$

$$E_a = 1.1 \pm 0.2 \text{ kJ mol}^{-1}),$$

where R is the gas constant.

Figure 10b shows the Arrhenius plot of T_1 , where the contribution of the lattice vibration was subtracted.

The relaxation can be readily attributed to the motion of Py derived from the two envelope conformations, where the decrease in T_1 during the cooling process clearly indicates that the frequency of the motion approaches the NQR frequency (ca. 36 MHz) from the faster frequency region. It is important to note that Low-B and High-B, in which the motion of Py almost freezes as indicated by the SCXRD measurements, show no sign of such a T_1 drop. The NQR results provide strong evidence that the freezing of the motion triggers the transition.

Conclusion

In this study, we demonstrate, for the first time, rational control over stacking patterns using chemical modification through the investigation of the stacking patterns of 2D molecular assemblies in hydrogen-bonded cocrystals from an energetic viewpoint using experimental and computational methods. We note that hydrogen-bonded crystals are recently attracting attentions owing to their potential for proton dynamics to afford the intriguing physical properties such as ferroelectricity and protonic soliton.^[33]

We have prepared a series of hydrogen-bonded cocrystals composed of 2-pyrrolidone (Py) and anilic acids bearing different halogens ($X = \text{F}, \text{Cl}, \text{Br}, \text{and I}$). Among all the cocrystals, only **PyCA** showed structural phase transitions between the four polymorphs via reversible High-A \leftrightarrow Low-A and irreversible High-A \rightarrow Low-B \rightarrow High-B transitions. SCXRD and NQR experiments revealed that the intersheet intermolecular

interactions and molecular motion associated with the two conformations of Py are key factors in determining the overlapping patterns. Notably, the contribution of molecular motion is an apparently unique nature of organic system. At the same time, we found that the change in the overlapping patterns caused by halogen substitution originates from the changes in (1) the intersheet interactions associated with the atomic polarizability of the halogen and (2) the motion of Py associated with the intrasheet cavity size depending on the size of the halogen. It is noteworthy that the occurrence of structural phase transitions only in **PyCA** can be attributed to the moderate polarizability and cavity of the 2D sheets.

The approach demonstrated here; namely the strong intermolecular interactions (e.g., hydrogen bonds) serve to assemble building blocks, whereas the weak intermolecular interactions (e.g., π - π and lone pair $\cdots\pi$) tunable through chemical modifications determine their assembling patterns, can be applied to various systems, including other dimensional systems. The trapping or stabilizing of enthalpically unfavorable patterns by using an entropic gain related to molecular flexibilities also have high potential to be utilized in diverse systems. These findings possibly pave the way to practical tuning of the physical and chemical properties of a wide range of molecular materials.

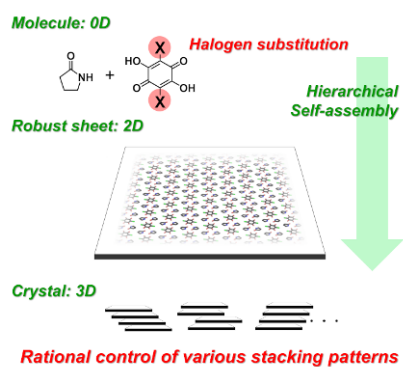
Acknowledgements

This work was supported by the ACCEL program (No. JPMJAC1501) of the Japan Science and Technology Agency (JST) and JSPS KAKENHI (No. 20H05623, 20H02708, and 19J23309). Synchrotron XRD experiments were supported by the Japan Synchrotron Radiation Research Institute (JASRI) (Proposal No. 2017A1468, 2017A1476, 2017B1379, 2019A1180, 2019B1380, 2020A1199, and 2020A1206).

Keywords: two-dimensional molecular compounds • intermolecular interactions • hydrogen bonds • molecular dynamics • polymorphism

- [1] a) *Extended Linear Chain Compounds*, (Ed.: J. S. Miller), Plenum Press, New York, **1982** (Vol. 1, 2), **1983** (Vol. 3); b) *Electronic Structure and Electronic Transitions in Layered Materials*, (Ed.: V. Grasso), D. Reidel Publishing, Dordrecht, **1986**; c) G. R. Desiraju, *Angew. Chem. Int. Ed.* **1995**, *34*, 2311–2327; d) B. Moulton, M. J. Zaworotko, *Chem. Rev.* **2001**, *101*, 1629–1658.
- [2] a) J. Bernstein, *Polymorphism in Molecular Crystals*, 2nd Ed., Oxford University Press, New York, **2020**; b) J. N. Israelachvili, *Intermolecular and Surface Forces*, 3rd Ed., Academic Press, New York, **2011**; c) J. Nyman, G. M. Day, *CrystEngComm* **2015**, *17*, 5154–5165; d) C. B. Aakeröy, M. Fasulo, N. Schultheiss, J. Desper, C. Moore, *J. Am. Chem. Soc.* **2007**, *129*, 13772–13773; e) R. Banerjee, R. Mondal, J. A. K. Howard, G. R. Desiraju, *Cryst. Growth Des.* **2006**, *6*, 999–1009.
- [3] a) J. A. Zerkowski, J. C. MacDonald, C. T. Seto, D. A. Wierda, G. M. Whitesides, *J. Am. Chem. Soc.* **1994**, *116*, 2382–2391; b) S. Palacin, D. N. Chin, E. E. Simanek, J. C. MacDonald, G. M. Whitesides, M. T. McBride, G. T. R. Palmore, *J. Am. Chem. Soc.* **1997**, *119*, 11807–11816; c) D. N. Chin, G. T. R. Palmore, G. M. Whitesides, *J. Am. Chem. Soc.* **1999**, *121*, 2115–2122.
- [4] R. T. Paine, C. K. Narula, *Chem. Rev.* **1990**, *90*, 73–91.
- [5] G. H. Han, D. L. Duong, D. H. Keum, S. J. Yun, Y. H. Lee, *Chem. Rev.* **2018**, *118*, 6297–6336.
- [6] G. Chakraborty, I. H. Park, R. Medishetty, J. J. Vittal, *Chem. Rev.* **2021**, *121*, 3751–3891.
- [7] K. S. Novoselov, A. K. Geim, S. V. Morozov, D. Jiang, Y. Zhang, S. V. Dubonos, I. V. Grigorieva, A. A. Firsov, *Science* **2004**, *306*, 666–669.
- [8] K. Geng, T. He, R. Liu, S. Dalapati, K. T. Tan, Z. Li, S. Tao, Y. Gong, Q. Jiang, D. Jiang, *Chem. Rev.* **2020**, *120*, 8814–8933.
- [9] a) I. Naik, A. K. Rastogi, *Pramana* **2011**, *76*, 957–963; b) Y. Cao, V. Fatemi, S. Fang, K. Watanabe, T. Taniguchi, E. Kaxiras, P. Jarillo-Herrero, *Nature* **2018**, *556*, 43–50; c) Y. Cao, V. Fatemi, A. Demir, S. Fang, S. L. Tomarken, J. Y. Luo, J. D. Sanchez-Yamagishi, K. Watanabe, T. Taniguchi, E. Kaxiras, R. C. Ashoori, P. Jarillo-Herrero, *Nature* **2018**, *556*, 80–84.
- [10] I. Huskić, N. Novendra, D. W. Lim, F. Topić, H. M. Titi, I. V. Pekov, S. V. Krivovichev, A. Navrotsky, H. Kitagawa, T. Friščić, *Chem. Sci.* **2019**, *10*, 4923–4929.
- [11] W. Q. Tang, Y. J. Zhao, M. Xu, J. Y. Xu, S. S. Meng, Y. D. Yin, Q. H. Zhang, L. Gu, D. H. Liu, Z. Y. Gu, *Angew. Chem. Int. Ed.* **2021**, *60*, 6920–6925.
- [12] a) R. J. Davey, S. J. Maginn, S. J. Andrews, S. N. Black, A. M. Buckley, D. Cottier, P. Dempsey, R. Plowman, J. E. Rout, D. R. Stanley, A. Taylor, *J. Chem. Soc., Faraday Trans.* **1994**, *90*, 1003–1009; b) D. P. Karothu, J. Weston, I. T. Desta, P. Naumov, *J. Am. Chem. Soc.* **2016**, *138*, 13298–13306.
- [13] T. Sasaki, Y. Miyamoto, S. Takamizawa, *Cryst. Growth Des.* **2020**, *20*, 4779–4782.
- [14] a) C. A. Hunter, J. K. M. Sanders, *J. Am. Chem. Soc.* **1990**, *112*, 5525–5534; b) R. Thakuria, N. K. Nath, B. K. Saha, *Cryst. Growth Des.* **2019**, *19*, 523–528.
- [15] T. J. Mooibroek, P. Gamez, J. Reedijk, *CrystEngComm* **2008**, *10*, 1501–1515.
- [16] M. Nishio, *CrystEngComm* **2004**, *6*, 130–158.
- [17] a) *Hydrogen Bonding—New Insights*, (Ed.: S. J. Grabowski), Springer, Dordrecht, **2006**; b) Y. Maréchal, *The Hydrogen Bond and the Water Molecule: The Physics and Chemistry of Water, Aqueous and Bio Media*, Elsevier, Amsterdam, **2007**; c) T. Steiner, *Angew. Chem. Int. Ed.* **2002**, *41*, 48–76.
- [18] a) J. C. MacDonald, G. M. Whitesides, *Chem. Rev.* **1994**, *94*, 2383–2420; b) L. J. Williams, B. Jagadish, S. R. Lyon, R. A. Kloster, M. D. Carducci, E. A. Mash, *Tetrahedron* **1999**, *55*, 14281–14300; c) L. J. Williams, B. Jagadish, M. G. Lansdown, M. D. Carducci, E. A. Mash, *Tetrahedron* **1999**, *55*, 14301–14322; d) R. Takasawa, I. Yoshikawa, K. Araki, *Org. Biomol. Chem.* **2004**, *2*, 1125–1132; e) K. Sada, K. Inoue, T. Tanaka, A. Tanaka, A. Epergyes, S. Nagahama, A. Matsumoto, M. Miyata, *J. Am. Chem. Soc.* **2004**, *126*, 1764–1771; f) B. Gong, C. Zheng, E. Skrzypczak-Jankun, Y. Yan, J. Zhang, *J. Am. Chem. Soc.* **1998**, *120*, 11194–11195; g) B. Gong, C. Zheng, H. Zeng, J. Zhu, *J. Am. Chem. Soc.* **1999**, *121*, 9766–9767; h) J. A. Zerkowski, C. T. Seto, D. A. Wierda, G. M. Whitesides, *J. Am. Chem. Soc.* **1990**, *112*, 9025–9026; i) J. A. Zerkowski, C. T. Seto, G. M. Whitesides, *J. Am. Chem. Soc.* **1992**, *114*, 5473–5475; j) J. A. Zerkowski, G. M. Whitesides, *J. Am. Chem. Soc.* **1994**, *116*, 4298–4304; d) J. A. Zerkowski, J. P. Mathias, G. M. Whitesides, *J. Am. Chem. Soc.* **1994**, *116*, 4305–4315; k) V. A. Russell, M. C. Etter, M. D. Ward, *J. Am. Chem. Soc.* **1994**, *116*, 1941–1952; l) V. A. Russell, C. C. Evans, W. Li, M. D. Ward, *Science* **1997**, *276*, 575–579; m) O. Ermer, *J. Am. Chem. Soc.* **1988**, *110*, 3747–3754.
- [19] a) K. Gotoh, H. Ishida, *Acta Cryst.* **2011**, *C67*, o500–o504; b) M. Donoshita, M. Hayashi, R. Ikeda, Y. Yoshida, S. Morikawa, K. Sugimoto, H. Kitagawa, *Chem. Commun.* **2018**, *54*, 8571–8574.
- [20] T. Akutagawa, H. Koshinaka, D. Sato, S. Takeda, S. Noro, H. Takahashi, R. Kumai, Y. Tokura, T. Nakamura, *Nat. Mater.* **2009**, *8*, 342–347.
- [21] S. Hayami, K. Murata, D. Urakami, Y. Kojima, M. Akita, K. Inoue, *Chem. Commun.* **2008**, 6510–6512.
- [22] X. Su, F. Zuo, J. A. Schlueter, M. E. Kelly, J. M. Williams, *Phys. Rev. B* **1998**, *57*, R14056–R14059.
- [23] A. Bondi, *J. Phys. Chem.* **1964**, *68*, 441–451.
- [24] a) H. Wang, W. Wang, W. J. Jin, *Chem. Rev.* **2016**, *116*, 5072–5104; b) P. Politzer, J. S. Murray, *J. Comput. Chem.* **2018**, *39*, 464–471.
- [25] A. Gavezzotti, *J. Phys. Chem. B* **2002**, *106*, 4145–4154.
- [26] T. M. Miller, Polarizabilities of atoms and molecules, in *CRC Handbook of Chemistry and Physics*, 100th ed. (Ed.: J. R. Rumble) CRC Press, Boca Raton, FL, **2019**, pp 10–96–10–97.
- [27] In the temperature region higher than 298 K, we used the samples sealed in glass capillaries.
- [28] a) M.-P. Zhuo, Y.-C. Tao, X.-D. Wang, Y. Wu, S. Chen, L.-S. Liao, L. Jiang, *Angew. Chem. Int. Ed.* **2018**, *57*, 11300–11304; b) Y. Liu, H. Hu, L. Xu, B. Qiu, J. Liang, F. Ding, K. Wang, M. Chu, W. Zhang, M. Ma, B. Chen, X. Yang, Y. S. Zhao, *Angew. Chem. Int. Ed.* **2020**, *59*, 4456–4463.
- [29] a) B. Jeziorski, R. Moszynski, K. Szalewicz, *Chem. Rev.* **1994**, *94*, 1887–1930; b) T. M. Parker, L. A. Burns, R. M. Parrish, A. G. Ryno, C. D. Sherrill, *J. Chem. Phys.* **2014**, *140*, 094106.
- [30] a) T. P. Das, E. L. Hahn, *Nuclear Quadrupole Resonance Spectroscopy*, In Solid State Physics (Suppl. 1), Academic Press, New York, **1958**; b) A. Rigamonti, *Adv. Phys.* **1984**, *33*, 115–191.
- [31] a) Y. Tobu, R. Ikeda, T. A. Nihei, K. Gotoh, H. Ishida, T. Asaji, *Phys. Chem. Chem. Phys.* **2012**, *14*, 12347–12354; b) B. Nogaj, *Bull. Chem. Soc. Jpn.* **1988**, *61*, 549–556.
- [32] It should be noted that the estimation of the activation energy for the molecular motion of Py contains some uncertainty. We performed the fitting for High-A using the data below 270 K because there seems to exist another relaxation attributable neither to the lattice vibration nor to the molecular motion of Py at higher temperatures (we do not discuss it in detail here). In the temperature range (< 270 K), there is no range where the relaxation originates mainly from the lattice vibration, which results in the uncertainty in the estimation of the contribution of the lattice vibration. In this study, we used the fitting result of High-B to subtract the contribution of lattice vibration for High-A. It should be noted that the High-B data covers a wider temperature range compared to the Low-B data including the temperature range where the molecular motion was observed for High-A. Although the assumption that the contribution of lattice vibration for High-A is the same as that for Low-B leads to the different activation energies for the motion (see Figure S11), it is evident that our NQR measurements detected the motion of Py in High-A because the T_1 value steadily decreases as the temperature approaches the High-A → Low-B transition temperature (ca. 165 K) at which the motion of Py almost freezes as indicated by the SCXRD measurements.
- [33] a) S. Horiuchi, S. Ishibashi, *J. Phys. Soc. Jpn.* **2020**, *89*, 051009; b) A. S. Davydov, *Solitons in Molecular Systems*, 2nd Ed., Kluwer Academic Publishers, Dordrecht, **1991** (English translation); c) I. Takasu, T. Sugawara, T. Mochida, *J. Phys. Chem. B* **2004**, *108*, 18495–18499.

Entry for the Table of Contents



Rational control of the stacking patterns of molecular two-dimensional layers in a series of hydrogen-bonded cocrystals by a chemical modification is demonstrated. The effect of the chemical modification is discussed in terms of both the enthalpic and entropic contributions based on experimental and computational results.